Journal of King Saud University - Science 36 (2024) 103087

HOSTED BY

Contents lists available at ScienceDirect

Journal of King Saud University - Science

journal homepage: www.sciencedirect.com

Full Length Article

The impact of Bi^{3+} ions on magnetization, dielectric parameters, and conductivity of soft Mg-Cu ferrite nanoparticles

Hanaa Almaghamsi

Physics Department, College of Science and Art, King Abdulaziz University, POB 344, Rabigh 21911, Saudi Arabia

ARTICLE INFO

Keywords:
Nanoferrites
Bismuth
Magnetic properties
Dielectric properties
Conduction mechanism

ABSTRACT

This paper investigates the bismuth ions leverage on magnetic and dielectric features of magnesium–copper nanoferrites $Mg_{0.5}Cu_{0.5}Bi_xFe_{2-x}O_4$ (MCBF). The $Mg_{0.5}Cu_{0.5}Bi_{0.1}Fe_{1.9}O_4$ nanoferrite exhibits superior magnetic properties compared to the pure Mg-Cu sample. These properties include a higher magnetization of 31.31 emu/g, with an enhancing ratio of 1.50 %. Additionally, it demonstrates a higher initial permeability of 17.84, with an enhancing ratio of 55.12 %. Furthermore, their coercivity is lower at 59.90 Oe, with an enhancing ratio of 50 %. All MCBF nanoferrites exhibit a high-frequency response between 6.106 and 6.926 GHz, making them suitable for microwave technology. The dielectric parameters dispersion shows normal behavior at different frequencies and temperatures. As for dielectric parameters dependence on Bi content, it exhibited a peculiar manner. At a temperature of 297 K and a frequency of 50 Hz, the nanoferrite $Mg_{0.5}Cu_{0.5}Bi_{0.1}Fe_{1.9}O_4$ exhibits superior dielectric properties compared to the pure Mg-Cu sample. Specifically, it demonstrates the highest dielectric constant of 360.68, with an enhancing ratio of 125.97 %. Additionally, it displays the highest conductivity of 691.4 $\mu(\Omega.m)^{-1}$, with an enhancing ratio of 1543.23 %. Furthermore, the nanoferrite exhibits a lower dielectric loss of 6.49, with an enhancing ratio of 80.22 % compared to the pure Mg-Cu sample. The conduction mechanism of the $Mg_{0.5}Cu_{0.5}Bi_xFe_{2-x}O_4$ nanoferrites was determined by fitting the σ_{ac} results via the Jonscher power law. This conduction mechanism is attributed to correlated barrier hopping (CBH) model up to 473 K, followed by small polaron tunneling (SPT), which reaches higher temperatures. Hence, the $Mg_{0.5}Cu_{0.5}Bi_{0.1}Fe_{1.9}O_4$ nanoferrite has a remarkable magnetic and dielectric nature, which can be used as functional soft ferrite material in transformers and high-frequency electronic devices.

1. Introduction

The fast telecommunications and information technology development has generated a need for smaller, more cost-effective, and more efficient electronic gadgets, which provide a wide range of functions to make our lives easier. For this purpose, soft ferrites, which are applicable in several fields like memory devices, microwave absorbing materials, magnet recording media, computer components, transformer cores, etc., have been studied. (Akhtar et al., 2023). Magnesium-copper (Mg-Cu) soft ferrite stands out among other ferrites as being particularly intriguing because of the variety of Mg- and Cu-ferrite varieties inside it (Balamurugan et al., 2022). Mg-ferrites acquire high electrical resistivity $\sim 10^7\Omega$.cm, low Eddy current, low cost and coercivity (Mansour & Abdo, 2017; Mansour et al., 2017a), and Cu-ferrites acquire high permeability and electrical resistivity with moderate magnetization (Mansour et al., 2018a). Hence, in this paper, Mg-Cu ferrite with a formula $Mg_{0.5}Cu_{0.5}Fe_2O_4$ was selected to be our pristine sample to combine the required merits of magnetization, permeability, resistivity, and coercivity for proper applications of soft ferrites.

In recent years, several research groups have worked to modify the magneto-electrical characteristics of microferrites by replacing divalent, trivalent, and binary mixtures in response to the needs of specific applications. Liu et al. investigated the microstructure effects on the Zn-Mg-Cu ferrite's magnetic parameters and investigated their application for near-field communication (Liu et al., 2016). Yue et al., declared that Zn-Mg-Cu ferrites have good magneto-electrical features, making them appropriate materials for multilayer chip inductors with superior behavior and inexpensive (Yue et al., 2001). Mulushoa and Murali reported that $Mg_{0.5}Cu_{0.5}Fe_{1.5}Cr_{0.5}O_4$ nanoferrite could be beneficial for their possible usage in high-density recording media technology (Mulushoa & Murali, 2022). Kumar and Kumar declared that Ni-Cr substituted $MgFe_2O_4$ ferrite material is promising for recording

Peer review under responsibility of King Saud University.
E-mail address: Halmaghamsi@kau.edu.sa.

https://doi.org/10.1016/j.jksus.2023.103087
Received 8 July 2023; Received in revised form 18 November 2023; Accepted 29 December 2023
Available online 31 December 2023

materials (Kumar & Kumar, 2016). Junaid et al. reported that Bi^{3+} substitution into different ferrite systems could increase the magnetization and decrease dielectric loss (Junaid et al., 2020). Choudhari and Rewatkar declared that Bi^{3+} ions-doped lead hexaferrite are appropriate for wide applications like permanent magnets and high-density magnetic recording media (Choudhari & Rewatkar, 2022). Pan et al. investigated the structural and magnetic properties of Bi^{3+} ion doped Ni–Cu–Co nano ferrites and declared their low magnetic properties (Pan et al., 2019). Alqarni et al. (Alqarni et al., 2022) stated that the diamagnetic Bi^{3+} can nestle in the two sites of spinel lattice (tetrahedral and octahedral) and improve resistivity and magnetic parameters. The prime intent of the current paper is to increase magnetization (M_S), permeability, and resistivity decrease coercivity (H_C) and decrease electric loss of the pristine $Mg_{0.5}Cu_{0.5}Fe_2O_4$ ferrites to obtain a remarkable soft ferrite material. For this purpose, we aimed to improve in the $Mg_{0.5}Cu_{0.5}Fe_2O_4$ ferrite system by substituting the Fe^{3+} with Bi^{3+} ions, based on the declared influence of Bi^{3+} ions on different ferrite systems. Hence, the magnetic and dielectric features of the $Mg_{0.5}Cu_{0.5}Bi_xFe_{2-x}O_4$ nanoferrites were investigated. In the previous paper (Almaghamsi and Basfer, 2022), the nanoferrite $Mg_{0.5}Cu_{0.5}Bi_{0.1}Fe_{1.9}O_4$ was found to have the highest photocatalytic efficiency (95.81 %) for the elimination of rhodamine B from effluent via the study of the optical and photocatalytic characteristics of the $Mg_{0.5}Cu_{0.5}Bi_xFe_{2-x}O_4$ system. Now, we have completed our investigation of these $Mg_{0.5}Cu_{0.5}Bi_xFe_{2-x}O_4$ nanoferrites by determining their magnetic, dielectric, and electric modulus spectroscopy features for proper soft ferrite applications.

2. Experimental

The sol–gel auto-combustion method was utilized to prepare the $Mg_{0.5}Cu_{0.5}Bi_xFe_{2-x}O_4$ ferrites samples (x = 0.0, 0.02, 0.04, 0.06, 0.08 and 0.1); which labeled MCBF0 ($Mg_{0.5}Cu_{0.5}Fe_2O_4$), MCBF1 ($Mg_{0.5}Cu_{0.5}Bi_{0.02}Fe_{1.98}O_4$), MCBF2 ($Mg_{0.5}Cu_{0.5}Bi_{0.04}Fe_{1.96}O_4$), MCBF3 ($Mg_{0.5}Cu_{0.5}Bi_{0.06}Fe_{1.94}O_4$), MCBF4 ($Mg_{0.5}Cu_{0.5}Bi_{0.08}Fe_{1.92}O_4$) and MCBF5 ($Mg_{0.5}Cu_{0.5}Bi_{0.1}Fe_{1.9}O_4$), respectively (Almaghamsi and Basfer, 2022). The chemicals exploited for the MCBF synthesis are metal nitrates of magnesium, copper, bismuth, and iron besides citric acid and ammonium solution. These nitrates and citric acid were dispersed in distilled water with a 1:1 M ratio; then, the solution pH values were altered to 7 by ammonium solution. At a temperature of 320 °C, the solvent completely evaporated during combustion, leaving behind dry ash powder. Previous work revealed the results of x-ray diffraction (XRD) and field emission scanning electron microscope (FESEM) analyses of these MCBF samples with their optical and photocatalytic properties (Almaghamsi and Basfer, 2022). The prepared MCBF nanoferrites' crystallite size was in the range 29.75 to 44.87 nm. Fourier transform infrared (FTIR) spectra for all MCBF nanoferrites were performed in the frequency span of 200–4000 cm^{-1} on a desktop FTIR model of "Bruker Tensor 27″ spectrometer". The magnetic parameters of the MCBF ferrite nanoparticles were measured via a vibrating sample magnetometer (VSM) Lake Shore 7410 USA device. The dielectric parameters and modulus of the MCBF ferrite samples were discussed with the help of a Hioki impedance analyzer model IM3570 with a measurement frequency of 4 Hz to 5 MHz at temperatures ranging from room temperature (RT = 297 K) to high temperature (T = 773 K).

3. Results and discussion

3.1. FTIR analysis

Fig. 1 displays transmittance data for MCBF nanoferrites within the frequency range 200–2000 cm^{-1}, obtained by FTIR spectroscopy for studying the interaction of IR with the MCBF nanoparticles. The FTIR spectra manifest the existence of the O–H group and residual water in

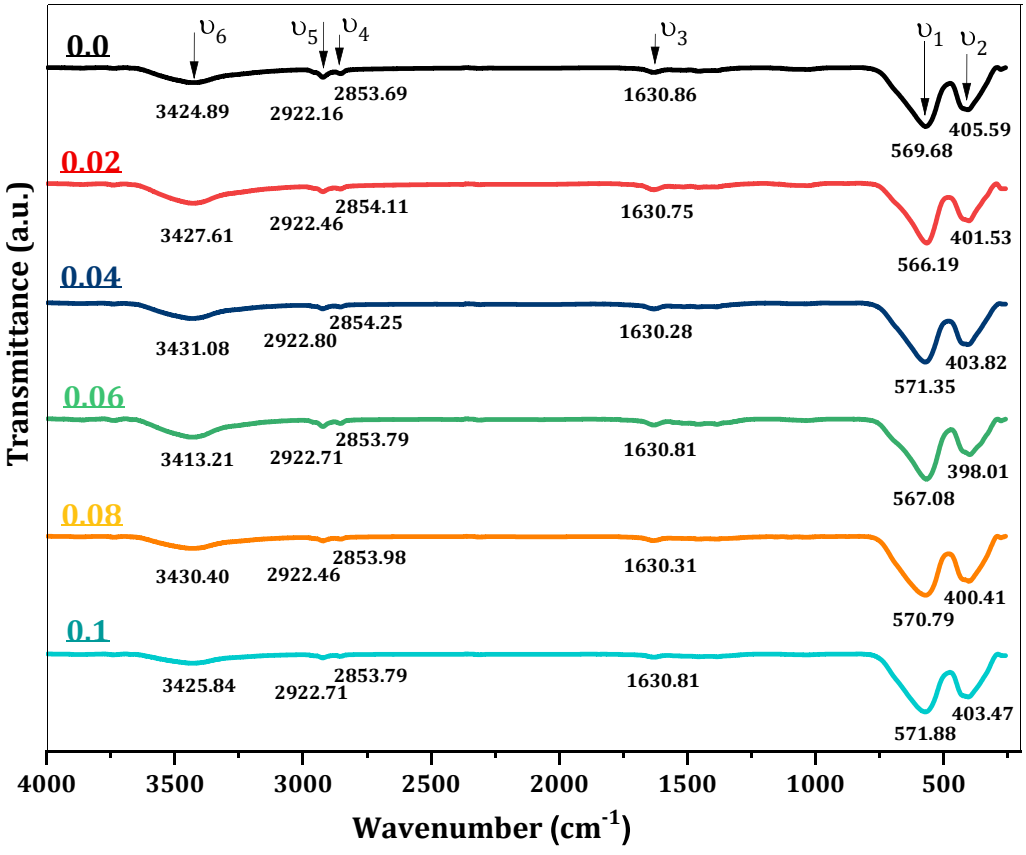

Fig. 1. FTIR diffractograms of $Mg_{0.5}Cu_{0.5}Bi_xFe_{2-x}O_4$; x = 0.0, x = 0.02, x = 0.04, x = 0.06, x = 0.08 and x = 0.1 nanoferrites.

the MCBF samples, which are the main reasons for the bands around (υ_3) 1630, (υ_4) 2854, (υ_5) 2922, and (υ_6) 3425 cm^{-1} (Harqani and Basfer, 2022). All the spectra acquire the vibrational bands of metal–oxygen (M−O) bonds at tetrahedral (A) and octahedral (B) positions of MCBF spinels (Ahmed et al., 2011). Band υ_1 is between 566.19 and 571.88 cm^{-1}, corresponding to the A site stretching mode (Abdo et al., 2021). The second one, υ_2, has values between 398.01 and 405.59 cm^{-1}, related to the B site stretching mode (Abdo and Sadeq, 2022). Variations in the lengths of the Fe^{3+}–O^{2-} bonds due to differences in A and B coordination are the source of the discrepancy between υ_1 and υ_2 values (Abdo and Sadeq, 2021). Redistributions of cations between A and B sites are inferred from the non-constant values of υ_1 and υ_2 with increasing Bi^{3+} concentration (Al-Bassami et al., 2020). It is observed that the band ν_1 moves to a lower wavenumber value for Bi^{3+}; meanwhile, υ_2 shifts to a higher wavenumber value. Spinel distortion occurs because of ion radius changes, involving Bi^{3+} ions and the rearrangement of Fe^{3+}, Cu^{2+}, and Mg^{2+}. The Bi^{3+} radius is large (1.03 Å), so it is inclined to nestle the B-sites. At the same time the Mg^{2+} radius (0.72 Å) is greater than that of the Fe^{3+} ion (0.645 Å) and Cu^{2+} (0.57 Å). Therefore, Bi^{3+} ions filling B-sites will initiate some Mg^{2+} ions to move to A-sites, and specified Fe^{3+} and Cu^{2+} ions will migrate from A-sites to B-sites to improve the strain. Hence, a growing number of Mg^{2+} ions in A-sites increases the ionic radii of the A-sites and leads to the move to higher wavenumber value, with an increasing number of Cu^{2+} ions in B-sites decreasing the ionic radii of the B-sites and lead to the shift to lower wavenumber. Fig. 1 illustrates the values of all these bands for all MCBF nanoferrites. The lack other bands proves that all MCBF nanoferrites have a single spinel structure.

3.2. Magnetic study

To determine the dominant magnetic phase and parameters, a VSM was employed to record the direct current (DC) magnetic field-dependent hysteresis loops of MCBF nanoferrites at RT. Fig. 2 shows the M(H) loops with zoomed-in depiction recorded via a field of ± 20 kOe. All the MCBF nanoferrites have ferrimagnetic characteristics with notable diverse magnitudes of saturation magnetization (M_S), coercivity (H_C), and remnant (M_r); see Table 1. M_S has a peculiar trend; it decreased gradually from 30.84 at MCBF0 to 27.60 emu/g for MCBF3 and increased, reached 30.15 and 31.31 emu/g for MCBF4 and MCBF5, respectively. This behavior can be justified as follows. Firstly, this decreasing behavior is a logical result of the substitution process of the Bi^{3+} ion with a magnetic moment of $3\mu_B$ at the expense of the higher

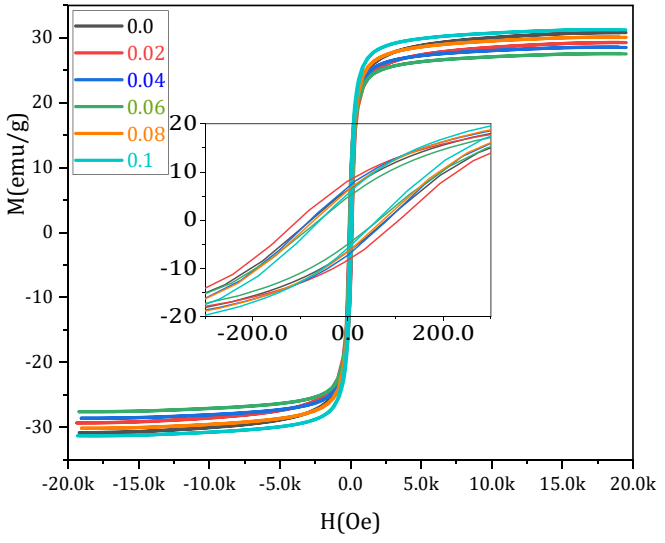

Fig. 2. VSM of all the MCBF nanoferrites with zoomed-in picture.

magnetic ion Fe^{3+} of $5\mu_B$ (Kumar and Kumar, 2016). Indeed, the largest Bi^{3+}ions (1.03 Å) (Shannon, 1976) can nestle in the largest B positions. Néel's two-sublattice ferrimagnetism model states that ions on the A and B sublattices have collinear spins and anti-parallel magnetic moments. Then, the lattice's net magnetic moment is the difference between the magnetic moments of the B and A sub-lattices $\mu_B = |\mu_{B(B)} - \mu_{B(A)}|$ (Ahmed et al., 2013). So, by doping Bi^{3+} ions instead of Fe^{3+} ones in the B sites, the net magnetic moment decreases, and then M_S also decreases. Secondly, for significant content of Bi^{3+}, i.e., MCBF4 and MCBF5 nanoferrites, M_S introduces an increment behavior which can be assigned for cations redistribution of nonmagnetic Mg ($0\mu_B$) (Mansour et al., 2017a), and magnetic Cu ($1\mu_B$) (Mansour et al., 2018a) between A and B sites, as seen above in FTIR results. Increasing Bi^{3+} ions in B sites at the expense of Fe^{3+} ions forces some of the large Mg (0.72 Å, 0μB) to migrate into the site, which in turn forces some small Cu (0.57 Å, 1μB) to migrate into B sites. This process decreases the A sites' magnetic moment and increases the B sites' magnetic moment, increasing the overall M_S. Hence, Bi^{3+} ions substitution can tune the magnetization of pristine Mg-Cu ferrite nanoparticles. Nanoparticles have a distinguished surface-to-volume ratio; hence, the number of dangling bonds or spin tilting effects at the nanoparticles' surface rises, decreasing the allied magnetic moments number across the particles. Fig. 3 manifests the nearly direct relation between magnetization and the size of MCBF ferrite nanoparticles (Abdo and El-Daly, 2022). Also, the magnetization of the sample MCBF5 is enhanced with an improved ratio of 1.51 % compared to the pristine sample. Thus, the first aim of this paper, enhancing the magnetization with Bi^{3+} doping, is achieved. Also, the remnant magnetization is enhanced by decreasing its value compared with the pristine sample. The characteristic sample MCBF5 has a M_r value of 5.61 emu/g, whereas the pristine sample has M_r value of 6.36 emu/g. Hence, the remnant magnetization is decreased with a decreasing ratio of 11.83 % to the pristine sample. This was the second aim of this paper, which was also achieved.

The squareness ratio (SQR) is a dimensionless quantity equals M_r/M_S (Mansour et al., 2021a), which notifies principally about the magnetic domain nature of the investigated magnetic samples behaving as ferri- or ferromagnetic material (Alqarni et al., 2022). According to Stoner-Wohlfarth's theory, a value of 0.5 is necessary for nanoparticles' SQR to acquire a single-domain nature with uniaxial symmetry. The calculated SQR values of the investigated MCBF nanoferrites are within the range of 0.18 and 0.28. Hence, it is concluded that our prepared MCBF samples are ferrimagnetic nanoparticles with multi-domain nature. Another important magnetic parameter is the magnetic moment per chemical formula (η_B), which depends mainly on the M_S, density (ρ), and molecular weight (MW) of each formula through the formula (Abdo et al., 2023):

$$\eta_M = \frac{(MW) \times M_S}{5585 \times \rho} \quad (1)$$

As expected, η_B has the same behavior of M_S and its values within the range 0.24 μ_B and 0.22 μ_B for all the MCBF nanoferrites; see Table 1. Observing the M_S, M_r, and SQR results, it is simple to deduce that the presence of Bi^{3+} ions positively adjust the magnetization data and achieve the required mission.

On the other hand, the H_C of the MCBF nanoferrites manifests a remarkable behavior within the range 105.61 and 59.90 Oe; see Table 1. As mentioned above, we aimed to decrease the H_C values through the Bi/Fe substitution process. H_C of the nanoferrite MCBF5 has the lowest value, 59.90 Oe, with an improving ratio of 50 %, compared to the pristine MCBF0 sample with 78.99 Oe. In fact, there are many reasons that govern H_C behavior, like substitution element, size of the nanoparticle, etc. The reason for decreasing coercivity to its lowest value has two justifications. The first one is that sample has the lowest M_S value; hence the required field to conquer this magnetization is also tiny, producing low H_C value. The second one is the particle size effect, where the relation between H_C and the nanomaterial size is an inverse one; see

Table 1
The saturation magnetization (M_S), remnant magnetization (M_r), squareness ratio (SQR), coercivity (H_C), anisotropy constant, magnetic moment per formula unit (μ_M), initial permeability (μ_i), microwave frequency (ω_M), and x-ray density (ρ) of the nanoferrites $Mg_{0.5}Cu_{0.5}Bi_xFe_{2-x}O_4$, x = 0.0, 0.02, 0.04, 0.06, 0.08, and 0.1.

x	M_S (emu.g^{-1})	M_r (emu.g^{-1})	SQR	H_C (Oe)	P (g/cm^3)	$\eta_M(\mu_B)$	K (erg/cm^3)	μ_i	ω_M (GHz)
0	30.84	6.36	0.21	78.99	5.07	0.239	2537.65	11.50	6.82
0.02	29.31	8.19	0.28	105.61	5.16	0.226	3224.74	11.26	6.49
0.04	28.61	7.04	0.25	80.90	5.23	0.221	2410.56	14.85	6.33
0.06	27.60	4.88	0.18	62.18	5.23	0.216	1787.68	13.28	6.11
0.08	30.15	6.33	0.21	72.22	5.22	0.239	2268.39	13.69	6.671
0.1	31.31	5.61	0.18	59.90	5.40	0.244	1953.52	17.84	6.93

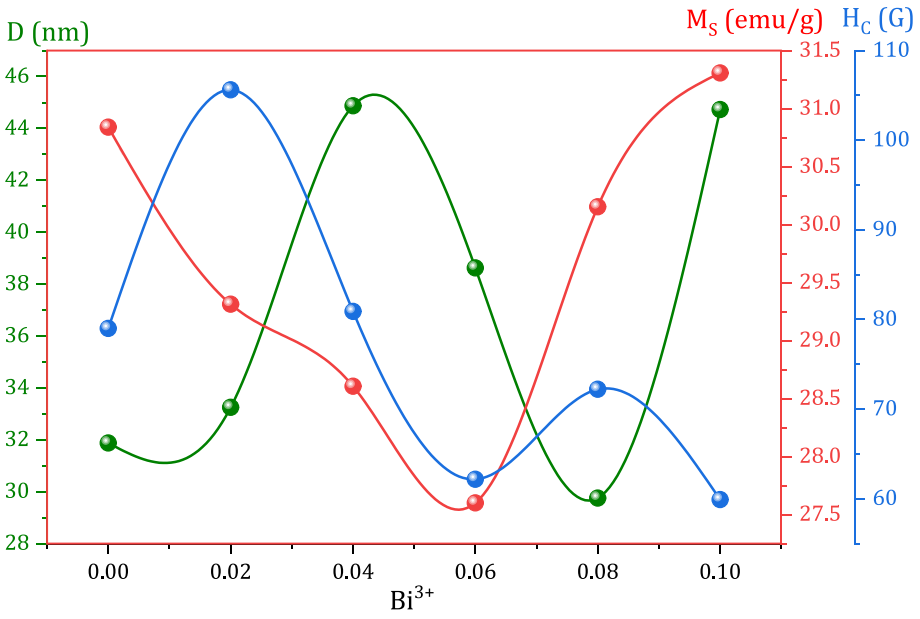

Fig. 3. Dependence of crystallite size (D_{nm}), magnetization (M_S), and coercivity (H_C) on Bi^{3+} content for all MCBF nanoferrites.

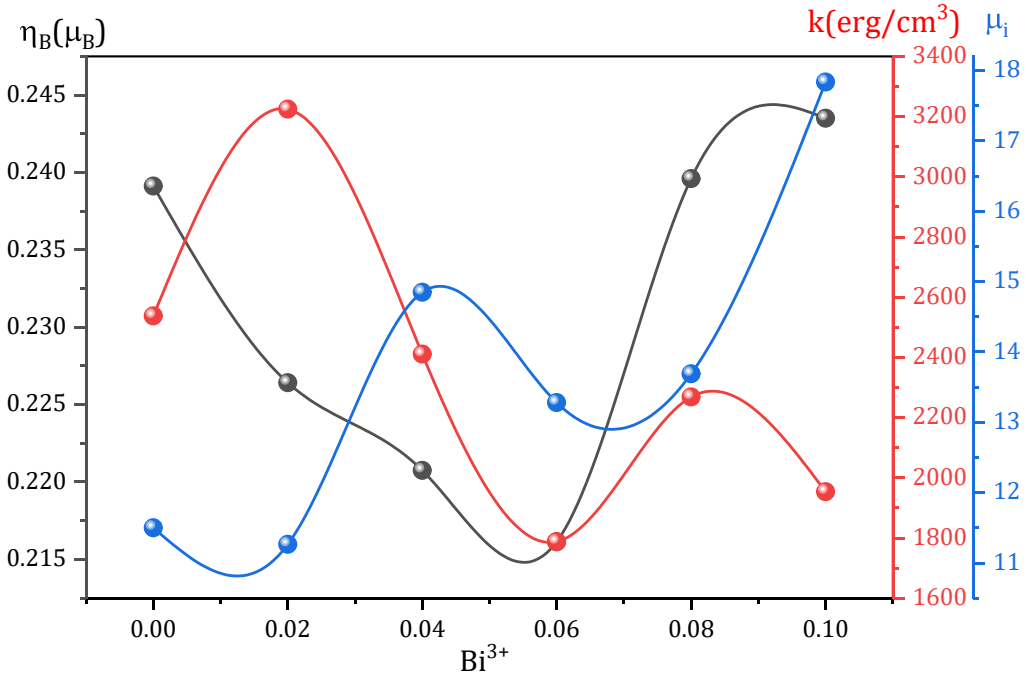

Fig. 4. Dependence of magnetic moment per formula unit (η_M), anisotropy constant (k), and initial permeability (μ_i) on Bi^{3+} content for all MCBF nanoferrites.

Fig. 3. Many authors reported an analogous inverse relation between H_C and particle size (Mansour et al., 2021b; Mansour et al., 2021c; Ali et al., 2021). Additionally, there are other magnetic parameters based on M_S, H_C, and crystallite size (D), anisotropy constant (k), and initial permeability (μ_i) can be determined through the following relations (Abdo and El-Daly, 2021; Abdo et al., 2022), and listed in Table 1.

$$k = \frac{M_S \times H_C}{0.96} \tag{2}$$

$$\mu_i = \frac{M_S^2 \times D}{k} \tag{3}$$

Fig. 4 displays the dependance of $\eta_B, \mu_i,$ and$k$ on Bi^{3+} content. k performance is ruled by both M_S and H_C values but takes the general behavior of H_C. Basically, magnetic anisotropy refers to the phenomenon whereby the magnetic properties of a ferrite material exhibit a dependency on the direction. Therefore, the nature of magnetic anisotropy plays a significant role in deciding whether a certain magnetic material is appropriate for a particular application. The significance of magnetic anisotropy is particularly apparent in both soft and hard magnetic materials. Due to the direct relationship between magnetic anisotropy and coercivity, soft magnetic materials typically exhibit minimal magnetic anisotropy. As seen k augmented for the nanoferrite MCBF1 (3224.74 erg/cm^3) and then generally decreased for further Bi doping. Hence Bi substitution decreases the crystalline anisotropy and generates samples that are easy to demagnetize. As for μ_i, it has a general increasing behavior, which increased from 11.50 for the nanoferrite MCBF0 to 17.84 for the nanoferrite CMCF5 with enhancing the ratio of 55.12 %. This increment confirms that the magnetic flux strengthens within the MCBF nanoferrite via the weaker magnetic ion Bi doping.

3.3. Dielectric studies

3.3.1. Frequency dependence of dielectric parameters

The dielectric constant (ε') quantifies a material's ability to retain energy in response to an alternating field. Using the following Eq. (Mansour et al., 2018a), the ε' values of all the MCBF nanoferrites were determined.

$$\varepsilon' = \frac{Ct}{\varepsilon_o A} \tag{4}$$

For each ferrite pellet, we have C, t, and A, which stand for its capacitance, thickness, and area, respectively; ε_o is the permittivity of free space. Fig. 5(a) shows the frequency dispersion of ε' of all the MCBF nanoferrites at RT, which exhibit the typical dispersion of all ferrite materials. The dielectric constant is mainly determined by the polarization types present in a substance. Ferrite materials were declared to include four polarization types at different frequencies: interfacial and orientational at lower frequencies (mHz to 1 MHz), ionic and electronic at higher frequencies (1 MHz to above GHz). The obtained dispersion in Fig. 5(a), interfacial and orientational types are the principal cause for the ε' behavior for all the MCBF samples. The ε' values of all the MCBF nanoferrites decrease with further increasing frequency. In fact, ε' has large values at a low frequency domain ($\leq$10 kHz), which reduces rapidly with increasing frequency. Then, in the range of 10 kHz $\leq$ f $\leq$ 5 MHz, ε' decreases slowly and becomes frequency-independent. It was reported that the ferrites' structure is composed of grains (G_S) and grain boundaries (GB_S) (Ahmed et al., 2013). Based on the Maxwell-Wagner model, in the range $\leq$ 10kH, polarization is generated by the buildup of charge carriers at the GB_S and produces high ε' values. The significant decrease in this area is due to the cessation of polarization since the charges cannot follow the frequency of the applied field. Regarding the range 10 kHz $\leq$ f $\leq$ 5 MHz, the ε' behavior is due to orientational polarization, where the dipoles' inability to follow the field frequency is the reason behind the ε' nearly constant values.

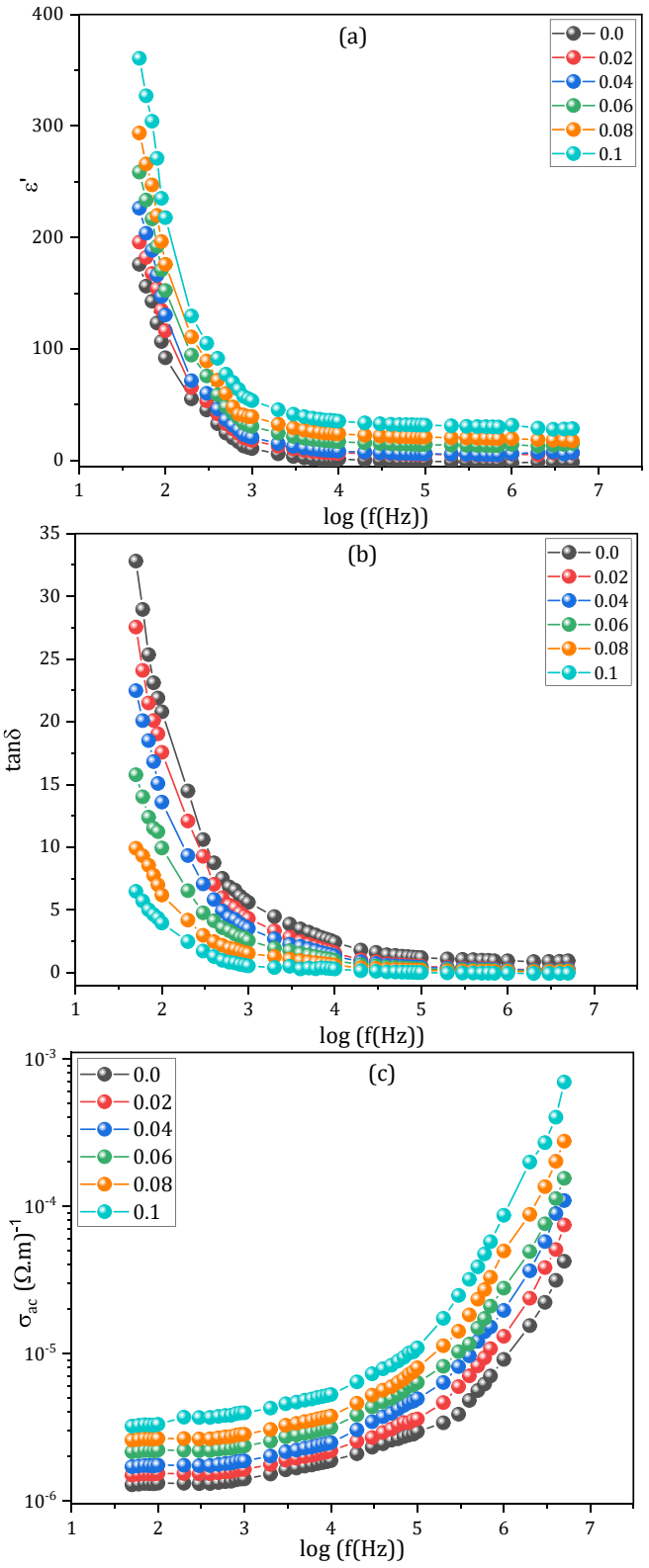

Fig. 5. (a-c): Frequency dependence of (a) dielectric constant ε', (b) dielectric loss tangent tanδ, and (c) conductivity σ_{ac} of all the MCBF nanoferrites at RT.

The dielectric loss tangent ($tan\delta$) is the consequence of the delayed action to the frequency, originating from diverse reasons. When a nanoferrite material is subjected to a field, the dipoles inside the material move closer and closer to the electrode. The dipoles' movement is then resisted by friction inside the ferrite material, leading to heat

production and dielectric loss (shown by *tanδ*). The *tanδ* readings of all MCBF samples are directly taken from the RLC apparatus. Fig. 5(b) shows the frequency dispersion of *tanδ* of all the MCBF nanoferrites at RT, which displays the characteristic dispersion of all ferrite materials. Obviously, *tanδ* has a rapid decay in the low frequency domain (≤10 kHz) followed by a slower decay within the span 10 kHz ≤ f ≤ 5 MHz. The operation of charge carrier hopping is slowed down by GB_S, leading to more absorption and more significant loss, especially at lower frequencies (Mansour et al., 2019a). Specifically, at low frequencies, the $Fe^{2+} \leftrightarrow Fe^{3+}$ exchange processes need more energy, which correlates with high resistive GB_S and leads to large tan values. On the other hand, the G_S function is more effective at high frequencies because charge carriers hop among ions in the octahedral sites. Consequently, *tanδ* decreases with frequency because absorption is less at higher frequencies, where electrons need less energy at higher frequencies (Mansour et al., 2018b).

Fig. 5(c) shows the frequency-dependence of alternating current (AC) conductivity (σ_{ac}) for the investigated MCBF samples at RT, where the σ_{ac} values were assessed using the formula.

$$\sigma_{ac} = 2\pi f \varepsilon_o \varepsilon' tan\delta \quad (5)$$

These results show that up to 10 kHz, σ_{ac} has small values but that beyond 10 kHz, significant increments occur. Multiple reports (Mansour et al., 2019b; Mansour et al., 2023) have established that ferrite's polarization process is like its conduction approach. Usually, the conduction route in ferrites arises mainly due to the exchange process of $Fe^{3+} \longleftrightarrow Fe^{2}$. As was previously noted, GB_S becomes further effective at lower frequencies, impeding these electron exchange processes and leading to lower values for the σ_{ac}. Whereas, at higher frequencies, the enhanced carrier exchange activities inside the G_S are responsible for the larger σ_{ac} values.

3.3.2. *Bi content dependence of dielectric parameters*

Fig. 6 shows the ε' values of all MCBF nanoferrites at RT and 50 Hz. It was noticed that the ε' value increased as the Bi^{3+} content increased. The nanoferrite MCBF5 has the optimum ε' value of 365.68 with an improving ratio of 125.97 % to the pristine MCBF0 nanoferrite, which has just an ε' value of 159.61. This remarkable behavior is justified as follows. Bi^{3+} replaced Fe^{3+} ions and occupied the B-sites, as mentioned above, forcing the B sites' iron ions to emigrate to the A sites. As a result, more Fe^{2+} and Fe^{3+} ions are in the A sites, and more electrons are hopping between $Fe^{2+} \leftrightarrow Fe^{3+}$ ions in the A sites. Therefore, the possibility of electron accumulation on the GB_S increased in polarization and ε' value.

As for σ_{ac} dependence on Bi^{3+} content, it has an increment behavior with further Bi doping, as seen in Fig. 6. The nanoferrite MCMF5 has an σ_{ac} value of 691.8 $\mu(\Omega.m)^{-1}$, which is an outstanding outcome compared to the pure MCBF0 sample, which acquires an σ_{ac} value of 42.1 $\mu(\Omega.m)^{-1}$. It is noteworthy that the conductivity was enhanced with an enhancing ratio of 1543.23 % via Bi doping. As stated before, the causes of dielectric constant are comparable to those of conductivity in ferrite materials. So, the proposed mechanism for interpreting the ε' results is also valid for explaining the σ_{ac} results. Moreover, Jacob et al. declared that the conductivity of Mg-Cd-Bi nanoferrites was enhanced via hoping between Bi^{2+} and Bi^{3+} at octahedral sites (Jacob et al., 2023). Hence, these two reasons are the motives for enhancing conductivity of the MCBF with further increasing Bi content.

Fig. 6 also shows the *tanδ* values for MCBF nanoferrites at RT and 50 Hz. Amazingly, it was noticed that the loss diminished gradually with the rise of the bismuth element, which is a wonderful result. Liu et al. summed up the dielectric losses caused in dielectric materials, which can be classified into intrinsic and extrinsic roles (Liu et al., 2023). Intrinsic losses are caused by the anharmonic interaction of the applied electric field with the phonon system. Extrinsic losses, on the other hand, relate to crystal structure properties such as density, grain boundaries, porosity, etc. Then, it was declared that the relation between the system density and dielectric losses is an inverse relationship. For our MCBF samples, the substitution process is a large molecular weight element (Bi = 208.9804 g/mol) instead of a small one (Fe = 55.845 g/mol). Therefore, it is normal for the density to increase with further increasing Bi^{3+} content, leading to a decrease in dielectric loss. Table 1 shows all the calculated values of the MCBF densities. The nanoferrite MCBF5 has

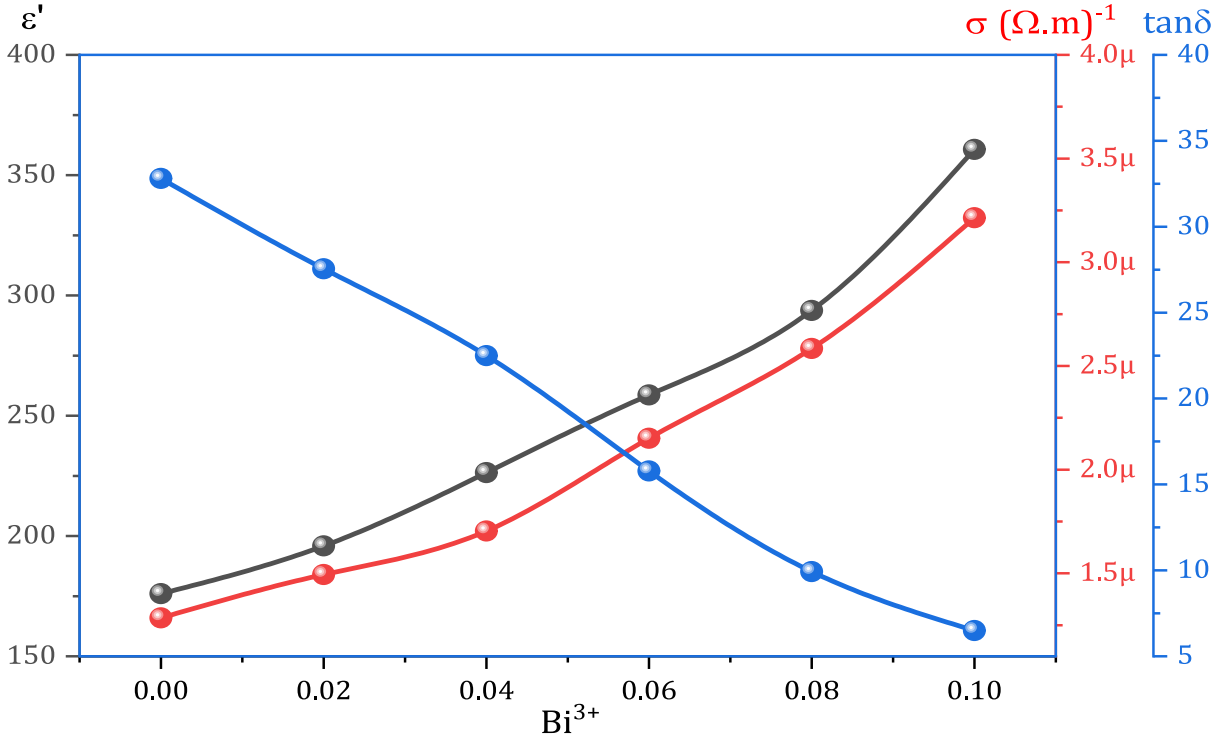

Fig. 6. Dependence of dielectric constant ε', conductivity σ_{ac}, and dielectric loss tangent tanδ on Bi^{3+} content for all MCBF nanoferrites at RT.

a loss of 6.49 with an enhancing ratio of 80.22 % compared with the nanoferrite MCBF0 loss of 32.81. Therefore, the dielectric parameters of the investigated CMBF nanoferrites can be remarkably tuned by Bi^{3+} ion doping.

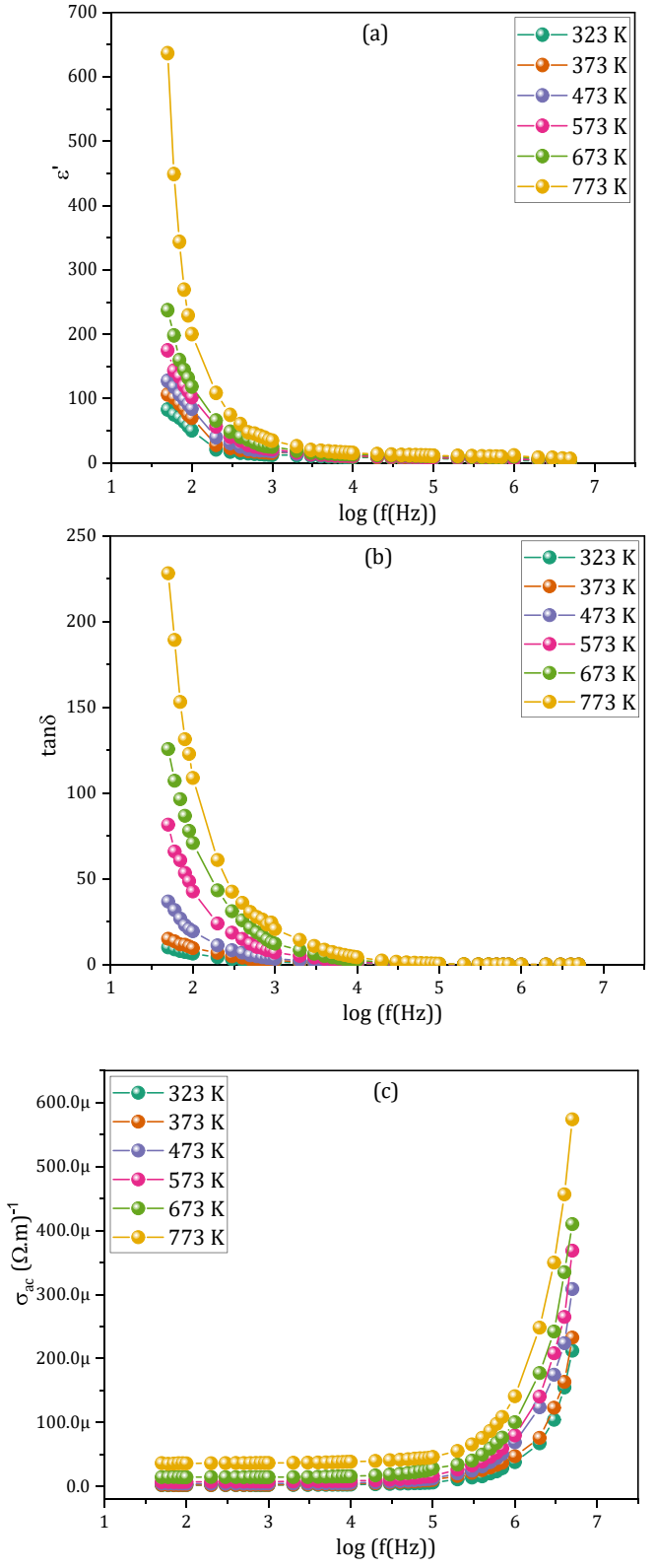

Fig. 7. (a-c): Frequency dependence of (a) dielectric constant ε', (b) dielectric loss tangent tanδ, and (c) conductivity σ_{ac} of all the MCBF nanoferrites different temperature.

3.3.3. *Temperature dependence of dielectric parameters*

Now, we will discuss the impact of temperature on the dielectric behavior of our MCBF nanoferrites. Fig. 7(a) manifests the ε' temperature-dependence of the nanoferrite MCBF4 (as a model for the reminder samples) at the frequency domain 50 Hz-5 MHz. The reminder MCBF nanoferrites have a similar general performance, which displays the typical response of all ferrite materials. The ε' values exhibit a growing disposition as the applied temperature rises. This trend may be explained by thermal energy, which causes the electrons to move more quickly and induces local dipoles to line up in the field direction, resulting in larger polarizations and ε' values (Mansour et al., 2018c).

Fig. 7(b) shows the σ_{ac} temperature-dispersion of the nanoferrite MCBF4 (as a model for the reminder samples) at the frequency range 50 Hz-5 MHz. The reminder MCBF nanoferrites have the same general behavior, which displays the typical response of all ferrite materials. When the applied temperature rises, σ_{ac} rises, which may be ascribed to the thermal energy that increases charge carrier mobility (Mansour et al., 2023). The charge carriers' exchanges are mainly through electron hopping between $Fe^{3+}\leftrightarrow Fe^{2+}$ and $Bi^{3+}\leftrightarrow Bi^{2+}$, besides the hole exchange between $Cu^{2+}\leftrightarrow Cu^{1+}$.

Fig. 7(c) shows the *tanδ* temperature-dependence of the nanoferrite MCBF4 (as a model for the reminder samples) at the frequency range 50 Hz-5 MHz. The reminder MCBF nanoferrites have the same general behavior, which can be understood as follows. Indeed, *tanδ* temperature-dependent behavior is primarily due to the existence of temperature-dependent charge carriers scattered throughout the ferrite material (Mansour et al., 2017b). Hence, the scattering of charge carriers through the mainly hopping of $Fe^{2+}\leftrightarrow Fe^{3+}$ and $Bi^{3+}\leftrightarrow Bi^{2+}$ besides exchange through the other divalent cation.

3.3.4. *Conduction mechanism*

As all other ferrite materials, σ_{ac} for all the MCBF samples at diverse temperatures and frequencies follows Jonscher law:

$$\sigma_{ac} = \sigma_{dc} + A\omega^{S} \tag{6}$$

where dc stands for dc conductivity, ω for angular frequency ($\omega = 2\pi f$), A for a particular parameter, and S for an exponent term with a value between 0.0 and 1.0, indicating that the migration of charge carriers. Jonscher power law fitting is shown in Fig. 8 for a typical plot of ac for the nanoferrite MCBF4. Our MCMF samples' conduction mechanism may be inferred from the S factor and its temperature dependency. Fig. 9 displays the S factor for all MCBF samples within the temperature range of 303 to 737 K. Elliott's results demonstrated when the S factor decreases with increasing temperature, the conduction can be attributed to the correlated barrier hopping (CBH) model of electrons. However, the conduction can be attributed to small polaron tunneling (SPT) when the S factor increases with increasing temperature. In fact, the term "small polaron" refers to an electron or hole that has been confined by its self-induced atomic (ionic) displacement field in an area of linear dimension ("radius") of the order of the lattice constant (Appel, 1968). This SP in a solid, can tunnel through a potential barrier to an unoccupied state in a neighboring state with energy conserved by a tunneling process. wo distinct temperature ranges can be identified: (I) spanning from 303 to 473 K, and (II) spanning from 473 to 737 K. The CBH model accurately predicts a decrease in S as the temperature increases in area I. On the other hand, in area II, the value of S increases as the temperature increases, which aligns with the expected result according to the SPT model. Accordingly, CBH and SPT models will govern the MCBF samples' conduction mechanism over temperatures in regions I and II.

4. Conclusion

The present study investigates the impact of bismuth on the magnetic and dielectric characteristics of $Mg_{0.5}Cu_{0.5}Bi_xFe_{2-x}O_4$ (MCBF) nanoferrites, where x ranges from 0.0 to 0.1. The saturation magnetization

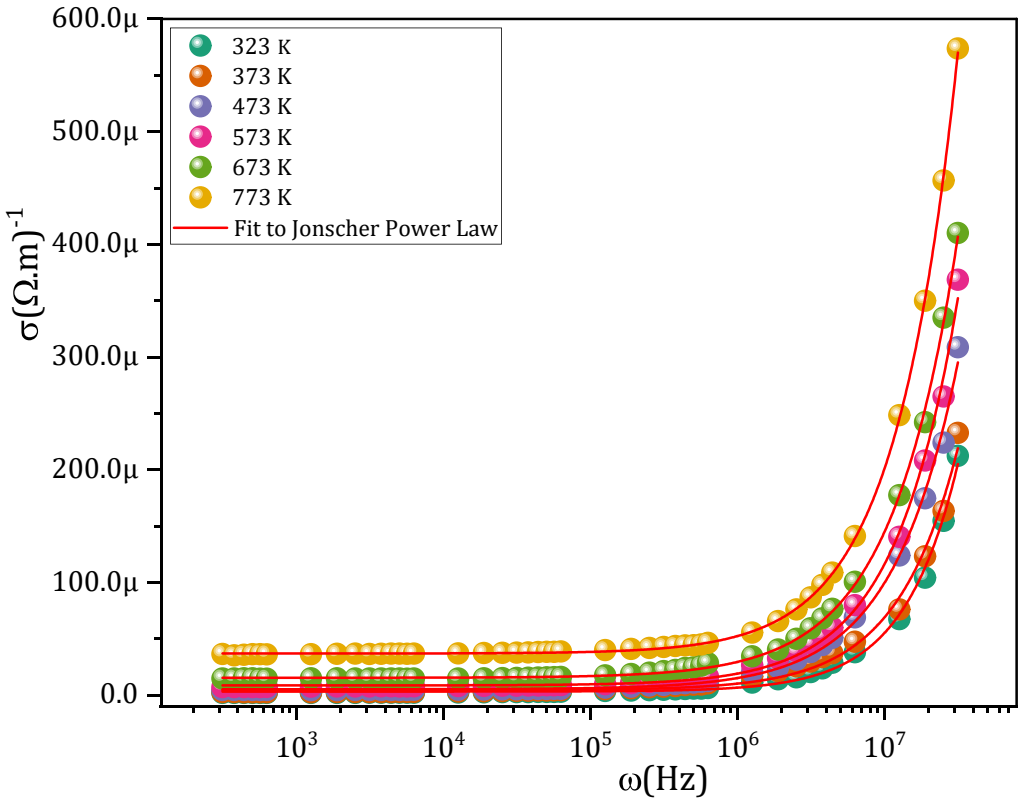

Fig. 8. A representative graph of σ_{ac} for the nanoferrite CMCF4, along with Jonscher power law fitting.

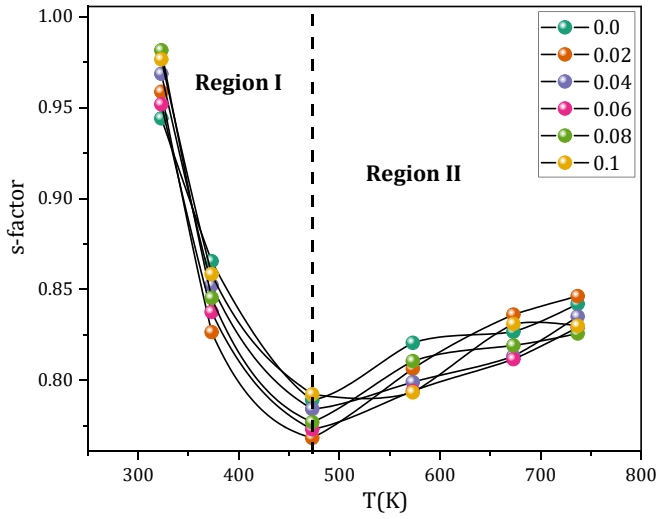

Fig. 9. *S* factor for all the MCBF nanoferrite.

exhibits an interesting pattern, wherein it demonstrates a steady reduction from 30.84 emu/g for MCBF0 to 27.60 emu/g for MCBF3. Subsequently, it undergoes an increase, reaching values of 30.15 emu/g and 31.31 emu/g for MCBF4 and MCBF5, respectively. This action was examined via the lens of two justifications. The H_C values of the nanoferrites in the MCBF exhibit a noteworthy behavior within the range of 105.61 and 59.90 Oe, leading to the classification of all samples as soft ferrite materials. Among the several nanoferrites that have been examined, it has been determined that the nanoferrite MCBF5 exhibits the most favorable characteristics. This is evidenced by its greatest values for M_S (31.307 emu/g), μ_i (17.84), and ε' (360.68), as well as its lower values for H_C (59.90 Oe), σ_{ac} (691.4 $\mu(\Omega.m)^{-1}$), and tanδ (6.49), when compared to the pure Mg-Cu nanoferrite. The conduction mechanism of the MCBF nanoferrites is governed by two distinct types in different temperature areas. In temperature region I, the conduction mechanism is characterized by the CBH type, while in temperature region II, it is governed by the SPT type.

Declaration of competing interest

The authors declare that they have no known competing financial interests or personal relationships that could have appeared to influence the work reported in this paper.

References

Abdo, M.A., El-Daly, A.A., 2021. Sm-substituted copper-cobalt ferrite nanoparticles: Preparation and assessment of structural, magnetic and photocatalytic properties for wastewater treatment applications. J. Alloy. Compd. 883, 160796.
Abdo, M.A., Sadeq, M.S., 2021. Covalency and Racah parameters of Fe3+ in Mn–Zn–Cr nanoferrites. Ceram. Int. 47 (20), 28237–28239.
Abdo, M.A., Sadeq, M.S., 2022. Impact of Cr3+ substitution on the nephelauxetic ratio and Racah parameter of Cr-Mn-Zn nanoferrites. Phys. Scr. 97 (1), 015804.
Abdo, M.A., Basfer, N.M., Sadeq, M.S., 2021. The structure, correlated vibrations, optical parameters and metallization criterion of Mn–Zn–Cr nanoferrites. J. Mater. Sci. Mater. Electron. 32 (12), 15814–15825.
Abdo, M.A., Mansour, S.F., Al-Bassami, N.S., Abu-Elsaad, N.I., 2022. Yttrium substituted Co–Cu–Zn nanoferrite: A synergetic impact of Y3+ on enhanced physical properties and photocatalysis. Ceram Int. 48 (11), 15314–15326.
Abdo, M.A., Al-Wafi, R., AlHammad, M.S., 2023. Highly efficient visible light driven photocatalytic activity of rare earth cerium doped zinc-manganese ferrite: Rhodamine B degradation and stability assessment. Ceram. Int. 49 (17), 29245–29258.
Ahmed, M.A., Mansour, S.F., Abdo, M.A., 2011. Characterization and dramatic variations of the magnetic properties of Cu-doped nanometric Co ferrite. Phys. Scr. 84 (5), 055602.
Ahmed, M.A., Mansour, S.F., Abdo, M.A., 2013. Improvement of the physical properties of novel (1− y) Co0.8Cu0.2Fe2O4+(y) SrTiO3 nanocomposite. Mater. Res. Bull. 48 (5), 1796–1805.
Akhtar, M., Hasan, M.S., Amin, N., Morley, N.A., Arshad, M.I., 2023. Tuning structural, electrical, dielectric and magnetic properties of Mg–Cu–Co ferrites via dysprosium (Dy3+) doping. J. Rare Earths.

Al-Bassami, N.S., Mansour, S.F., Abdo, M.A., 2020. The magneto-mechanical properties of cobalt substituted Mg-Zn nanoferrites. J. Supercond. Nov. Magn. 33 (10), 3077–3086.

Ali, T.M., Ismail, S.M., Mansour, S.F., Abdo, M.A., Yehia, M., 2021. Physical properties of Al-doped cobalt nanoferrite prepared by citrate–nitrate auto combustion method. J. Mater. Sci. Mater. Electron. 32 (3), 3092–3103.

Almaghamsi, H., Basfer, N.M., 2022. Structural, morphological and photocatalytic properties of Bi–Mg–Cu ferrites: Influence of the Bi: Fe ratio. Ceramics International.

Alqarni, A.N., Almessiere, M.A., Güner, S., Sertkol, M., Shirsath, S.E., Tashkandi, N., Baykal, A., 2022. Structural and magnetic properties of hydrothermally synthesized Bi-substituted Ni–Co nanosized spinel ferrites. Ceram. Int. 48 (4), 5450–5458.

Yue, Z., Zhou, J., Li, L., Wang, X., Gui, Z., 2001. Effect of copper on the electromagnetic properties of Mg–Zn–Cu ferrites prepared by sol–gel auto-combustion method. Mater. Sci. Eng. B 86 (1), 64–69.

J. Appel, "Polarons," in Solid State Physics, vol. 21, edited by F. Seitz, D. Turnbull, and H. Ehrenreich (Academic Press, New York, 1968), (1968), pp. 193–391.

Balamurugan, A., Priya, R.S., Chaudhary, P., Kumar, E.R., Indumathi, T., Srinivas, C., Sastry, D.L., 2022. Natural fuel assisted synthesis of Mg–Cu ferrite nanoparticles: Evaluation of structural, dielectric, magnetic and humidity sensing properties. Ceram. Int. 48 (4), 4874–4885.

Choudhari, Y.D., Rewatkar, K.G., 2022. Influence of Bi3+ ions substitution on structural, magnetic, and electrical properties of lead hexaferrite. J. Magn. Magn. Mater. 551, 169162.

Harqani, N.A., Basfer, N.M., 2022. The Role of Rare Earth (Y) Ions on the Structural, Magnetic and Mechanical Properties of Co–Mg Nanoferrites. J. Supercond. Nov. Magn. 35 (11), 3417–3429.

Jacob, J., Javaid, K., Amin, N., Ali, A., Mahmood, K., Ikram, S., Amami, M., 2023. The influence of lanthanum concentration on microstructural and electrical properties of Mg-Cd-Bi ferrite nanoparticles. Ceram Int. 49 (2), 1896–1901.

Junaid, M., Khan, M.A., Hashmi, Z.M., Nasar, G., Kattan, N.A., Laref, A., 2020. Structural, spectral, magnetic and dielectric properties of Bi substituted Li-Co spinel ferrites. J. Mol. Struct. 1221, 128859.

Kumar, N.S., Kumar, K.V., 2016. Effect of Bi3+ ion substitution on magnetic properties of cobalt nano ferrites prepared by sol-gel combustion method. Soft Nanosci. Lett. 6 (3), 37–44.

Liu, W., Yan, S., Zhang, Z., Jia, H., Luo, H., Chen, F., Nie, Y., 2016. The effects of microstructure on the magnetic properties of MgCuZn ferrites applied in near field communication. J. Alloy. Compd. 680, 328–332.

Liu, W., Kong, F., Zhao, Y., Jin, Y., Gao, J., Zhang, L., Li, S., 2023. Enhanced dielectric tunability and reduced dielectric loss tangent in the Mn-doped $BaTi_{0.8}Zr_{0.2}O_3$ ceramics. J. Alloy. Compd. 935, 167960.

Mansour, S.F., Abdo, M.A., 2017. Electrical modulus and dielectric behavior of Cr3+ substituted Mg–Zn nanoferrites. J. Magn. Magn. Mater. 428, 300–305.

Mansour, S.F., Al-Bassami, N.S., Afifi, M., Abdo, M.A., 2023. Y3+ substituting-adjusted mechanical, dielectric, and impedance properties of cobalt copper zinc nanoferrites for high frequency applications. J. Rare Earths 41 (10), 1597–1605.

Mansour, S.F.[a], Abdo, M. A., & El-Dek, S. I. (2017). Improvement of physico-mechanical properties of Mg–Zn nanoferrites via Cr^{3+} doping. Journal of Magnetism and Magnetic Materials, 422, 105-111.

Mansour, S. F.[b], Ahmed, M. A., El-Dek, S. I., Abdo, M. A., & Kora, H. H. (2017). Enhancement of the physical properties of novel (1−x) $NiFe_2O_4$+(x) Al_2O_3 nanocomposite. Applied Physics A, 123(7), 1-11.

Mansour, S. F.[a], Abdo, M. A., & Kzar, F. L. (2018). Effect of Cr dopant on the structural, magnetic and dielectric properties of Cu-Zn nanoferrites. Journal of Magnetism and Magnetic Materials, 465, 176-185.

Mansour, S. F.[b], Hemeda, O. M., Abdo, M. A., & Nada, W. A. (2018). Improvement on the magnetic and dielectric behavior of hard/soft ferrite nanocomposites. *Journal of Molecular Structure*, *1152*, 207-214.

Mansour, S. F. [c], Abdo, M. A., & Alwan, S. M. (2018). The role of Cr^{3+} ions substitution on structural, magnetic and dielectric modulus of manganese zinc nanoferrites. *Ceramics International*, *44*(7), 8035-8042.

Mansour, S. F.[a], Al-Hazmi, F., & Abdo, M. A. (2019). Relaxation time enhancement of cobalt zinc nanoferrites via Cr^{3+} doping. *Journal of Alloys and Compounds*, *792*, 626-637.

Mansour, S. F.[b], Dawood, A., & Abdo, M. A. (2019). Enhanced magnetic and dielectric properties of doped Co–Zn ferrite nanoparticles by virtue of Cr^{3+} role. *Journal of Materials Science: Materials in Electronics*, *30*(18), 17262-17275.

Mansour, S.F.[a], Karamany, M. M., Al-Wafi, R., El-Dek, S. I., Almossalami, H. A., & Abdo, M. A. (2021). The effective role of diamagnetic Pb ions in tailoring the magnetic and dielectric properties of $BiFeO_3$ nanomultiferroic. Journal of Materials Science: Materials in Electronics, 32(3), 3621-3637.

Mansour, S.F.[b], Al-Hazmi, F., AlHammad, M. S., Sadeq, M. S., & Abdo, M. A. (2021). Enhancing the magnetization, dielectric loss and photocatalytic activity of Co–Cu ferrite nanoparticles via the substitution of rare earth ions. Journal of Materials Research and Technology, 15, 2543-2556.

Mansour, S.F.[c], Zaher, H., Al-Wafi, R., Almossalami, H. A., & Abdo, M. A. (2021). Tuning of structural, magnetic and dielectric properties of $M_{0.45}La_{0.10}Fe_{2.45}O_4$;(M= Mn, Co, Cu, Mg and Zn) nanoparticles: effect of particle size and porosity. Journal of Materials Science: Materials in Electronics, 32(2), 1741-1758.

Mulushoa, S.Y., Murali, N., 2022. Comparison of Structural, dielectric and magnetic investigation of Cr3+ substituted Mg-Cu, Mg-Zn, and Mg-Ni ferrites system. Inorg. Chem. Commun. 145, 110033.

Pan, X., Sun, A., Han, Y., Zhang, W., Zhao, X., 2019. Structural and magnetic properties of Bi3+ ion doped Ni–Cu–Co nano ferrites prepared by sol–gel auto combustion method. J. Mater. Sci. Mater. Electron. 30, 4644–4657.

Shannon, R.D., 1976. Revised effective ionic radii and systematic studies of interatomic distances in halides and chalcogenides. Acta Crystallogr. Sect. A: Cryst. Phys., Diffr., Theor. Gen. Crystallogr. 32 (5), 751–767.